ORIGINAL PAPER

Simulation of wet and dry West African monsoon rainfall seasons using the Weather Research and Forecasting model

Imoleayo E. Gbode [1,2] · Kehinde O. Ogunjobi [1] · Jimy Dudhia [2] · Vincent O. Ajayi [1]

Abstract

This paper presents an evaluation of the Weather Research and Forecasting (WRF) model in simulating wet and dry West African monsoon (WAM) rainfall seasons. Three model experiments with varying selected microphysics (MP), cumulus convection (CU), and planetary boundary layer (PBL) schemes based on previous study were performed. Each of the model combinations is used to run four WAM seasons that consist of two wet (2008 and 2010) and two dry years (2001 and 2011). To investigate the behavior of WAM in the context of wet and dry years, the four seasons were used to compute composites of wet and dry WAM seasons in terms of rainfall amount. The analyses majorly focus on the rainfall composites relative to rainfall from Global Precipitation Climatology Project (GPCP) and Tropical Rainfall Measurement Mission (TRMM) as well as temperature, moisture, and atmospheric circulation fields with respect to NCEP reanalyses. This study documents significant sensitivity in simulation of the West African monsoon to the choices of the MP, CU, and PBL schemes. The simulation with the combination of WRF single moment 5 (WSM5) MP, Yonsei University (YSU) PBL, and new Simplified Arakawa-Schubert CU (WSM5-YSU-nSAS) shows good spatial distribution pattern of rainfall and the dynamics associated with the monsoon. Quantitatively, the combination shows less agreement in distinguishing the selected WAM seasons compared with the Goddard MP, Mellor-Yamada-Janjic PBL, and Betts-Miller-Janjić CU (GD-MYJ-BMJ) and the WSM5, Mellor-Yamada-Nakanishi-Niino 2.5 level and new Tiedtke CU (WSM5-MYNN-nTDK). Also, the dynamical structures of the wet and dry WAM circulation composites are reasonably reproduced in GD-MYJ-BMJ and WSM5-YSU-nSAS. The GD-MYJ-BMJ was able to distinguish between wet and dry years and thus underscores its potential to reproduce climate change signals in future work.

1 Introduction

The West African monsoon (WAM) is a complex atmospheric dynamics system of West African climate that provides about 75 to 90% of the total rainfall in the region (Hagos and Cook 2007). The West African climate system is however challenged by growing anthropogenic pressures together with the menace of climate change and variability that result in several environmental impacts. Such impacts could however modify atmospheric circulations (IPCC 2001, 2007; Hoegh-Guldberg et al. 2018) and thus have significant influence on variability of West

African monsoon intensity Hulme (1992), which could lead to flood during wet years and meteorological drought during dry years. Since the past few decades, the scientific and modeling communities have been channeling efforts to adequately understand the WAM variability by evaluating the capability of regional climate models (RCMs) to accurately represent such variability in model simulations (Sylla et al. 2009; Nikulin et al. 2012; Akinsanola et al. 2018). These campaigns have however provided reliable scientific findings relevant to inform sound decision-making and climate assessment necessary to help realize the sustainable development goals.

Several studies have analyzed both observed and modeled data to understand the causes of variability in precipitation and atmospheric circulation over the West African region. Most of these studies focus on the Sahel because of the unprecedented drought experienced in the region during the 1970s and 1980s (Christensen et al. 2007; Baines and Folland 2007). For example, Akinsanola and Zhou (2018) reported that most of the increasing rainfall over the central eastern Sahel is balanced by increasing vertical moisture flux and that the dynamic

✉ Imoleayo E. Gbode
   iegbode@futa.edu.ng

1   West African Science Service Center on Climate Change and
    Adapted Land Use (WASCAL), Federal University of Technology,
    Akure, Nigeria

2   Mesoscale and Microscale Meteorology Laboratory, National Center
    for Atmospheric Research, Boulder, CO, USA

component of the vertical moisture flux has the largest contribution to the observed increasing trend in the Sahel region. Another study theoretically argued that cold (warm) sea surface temperature anomalies located south of the West African region should favor a large (small) meridional gradient of entropy, a strong (weak) monsoon circulation, and wet (dry) conditions in the Sahel (Eltahir and Gong 1996). Other studies attributed the rainfall variability to changes in land surface (Charney et al. 1977) or atmospheric structures (Burpee 1972; Thorncroft and Blackburn 1999).

The mean date of rainfall pre-onset occurs in 14 May before the mean date of onset in 24 June when the WAM is fully developed (Sultan and Janicot 2003). The summer monsoon season dominates the months of June through to September. This gives rise to a lengthy dry season that is usually longer than the wet season. Areas in the southern part of the region experience two halves of rainfall periods during the rainy season; the longer half is generally observed from the end of April to July and the shorter from September to October. To the north of 10° N latitude, only one rainy season from July to September is experienced. The months of August and September characterize the late half of the rainy season when the monsoon circulation is fully developed and overrides the dynamics of the atmosphere.

This work evaluates the performance of Weather Research and Forecasting (WRF) model physics in simulating the wet and dry WAM with a focus on the microphysics (MP), planetary boundary layer (PBL), and cumulus convection (CU) schemes. Previous studies (e.g., Afiesimama et al. 2006; Flaounas et al. 2011; Sylla et al. 2010a; Xue et al. 2010; Nikulin et al. 2012; Hernández-Díaz et al. 2013; Im et al. 2014; Klein et al. 2015, among others) have made attempts to describe the key characteristics of the WAM in both global and regional climate models. These studies used some selected parameterization schemes to describe complex subgrid-scale processes that are not resolved by the model due to its horizontal resolution. Also, the schemes used are not exhaustive, and some, for example, the Kain-Fritsch convective scheme used in Nikulin et al. (2012), are known to produce too much rain (Gbode et al. 2018), and introduce uncertainties in the model outputs. This presents the need for the current study to perform further evaluation of the performance of the WRF model. A great concern is the difficulty in reproducing the rainfall distribution because of its strong variability at a wide range of temporal and spatial scales (Gallée et al. 2004; Sylla et al. 2010b). Further, the spatial and temporal rainfall distribution could vary greatly on intraseasonal, interseasonal, and interannnual scales depending on the behavior of the underlying atmospheric circulation that dominates during the WAM period. Out of many factors that modulate the characteristics of the WAM during wet and dry years, the cloud microphysical, planetary boundary layer, and convection processes will be studied through sensitivity experiments that compare two MP, three PBL, and three

CU schemes. These properties have been chosen because previous studies presented strong sensitivity in the model performance to the representation of subgrid-scale physical processes mostly cloud, convection, and planetary boundary layer activities (Klein et al. 2015; Gbode et al. 2018).

Recent studies using various versions of the WRF model have reported their efforts to improve the performance of the model in simulating the WAM and to understand the model behavior and sensitivity of the WAM to different model physics (e.g., Flaounas et al. 2011; Hagos et al. 2014; Noble et al. 2014; Li et al. 2015; Klein et al. 2015; Noble et al. 2017; Gbode et al. 2018). These studies have achieved substantial progress in terms of representing subgrid-scale physical processes, but there are however indications of model systematic errors, which underscore the need for improvements in the simulation of key processes. Due to the uncertainties inherent in the representation of subgrid-scale convective processes, Prein et al. (2013), among others, stressed the need to explicitly represent deep convection with a more realistic model dynamics, an approach challenged by huge computational cost. The current work builds on previous work by providing a detailed evaluation of existing and newly modified cumulus convection, planetary boundary layer, and microphysics schemes. The work portrays the capability of the WRF model to adequately simulate wet and dry WAM rainfall seasons. Section 2 gives a detailed description of the data and methods used. Section 3 presents and discusses the results, and conclusions are made in Section 4.

2 Data and methods

2.1 Model setup

The Advanced Research WRF model, version 3.8.1, is used at 20-km horizontal grid resolution to simulate different phases of the West African monsoon season. The simulations include selective wet (2008 and 2010) and dry (2001 and 2011) monsoon years. The WRF model physics used combines three parameterizations of subgrid-scale processes such as the CU, MP, and PBL effect (Table 1). These choices are based on an analysis of the model performance in some preliminary tests (Gbode et al. 2018). The selected physics are considered appropriate treatment for describing atmospheric processes such as (i) moisture and latent heat distribution through shallow and deep convective clouds; (ii) water vapor, cloud, and precipitation processes; and (iii) the evolution of atmospheric moisture, temperature, and wind profiles. The combined effect of the chosen physics determines the redistribution of moisture and heat at spatio-temporal scales aside from determining the cause of atmospheric phenomena in the West African region.

The moisture and temperature vertical fluxes are resolved by the PBL scheme at each grid point within the model's

Table 1 Regional physics parameterization schemes used in the study

Serial	Microphysics (MP)	Planetary boundary layer (PBL)	Cumulus convection (CU)
1	WRF single moment 5 (WSM5; Hong et al. 2004)	Yonsei University (YSU; Hong et al. 2006)	Betts-Miller-Janjić (BMJ; Janjić 1994, 2000)
2	Goddard (GD; Tao et al. 1989)	Mellor-Yamada-Janjić TKE (MYJ; Janjić 1994)	New Tiedtke (nTDK; Tiedtke 1989; Zhang et al. 2011)
3		Mellor-Yamada-Nakanishi-Niino 2.5 level TKE (MYNN; Nakanishi and Niino 2004, 2006)	New simplified Arakawa-Schubert (nSAS; Han and Pan 2011)

atmospheric column. The resulting vertical profiles feed into the MP and CU schemes at every model time step. Convective instabilities are released by the CU scheme in the model columns, which restricts the MP from generating unrealistic or erroneous grid-scale convection. The CU vertically redistributes the simulated moisture and heat to produce convective precipitation. On the other hand, the MP produces non-convective precipitation through the removal of surplus atmospheric moisture due to resolved saturation. The selected parameterization schemes (as shown in Table 2) use different algorithms to describe similar physical processes. However, for other physics like the land surface and radiation physics, the unified Noah land-surface model scheme (Chen and Dudhia 2001) and Rapid Radiative Transfer Model (RRTMG) schemes (Iacono et al. 2008), respectively, are kept constant in all simulations. Further details of the choice of physics can be found in Gbode et al. (2018).

The domain of the model simulation covers the region of active WAM activity (as shown in Fig. 1). The horizontal grid size of the model domain is 20 km. A vertical grid of 50 levels is used to ensure a good representation of deep vertical processes within the model atmospheric column of each grid scale. At every 6-h interval, the model gets atmospheric boundary conditions from the 0.75° ERA-Interim reanalysis (Dee et al. 2011) with initial soil moisture and temperature interpolated from the 1° resolution NCEP final analysis (NCEP FNL 2000; from the NCAR's Computational and Information Systems Laboratory Research Data Archive). FNL is used as the choice of soil initialization because its source model is more consistent with the unified Noah land-surface model. For grid point comparison, the model outputs were regridded to the observation grids using the first-order conservative remapping method (Jones 1999).

The West African region can be subdivided into three different climatic zones (as shown in Fig. 1): Guinea coast (4–8° N), Savannah (8–11° N), and Sahel (11–16° N), based on land use/land cover, climate, and ecosystem characteristics (Iloeje 1981; Omotosho and Abiodun 2007; Abiodun et al. 2013). Both observation and model data are employed to compute composites of wet and dry monsoon years. The composites are analyzed for each climatic zone to show the difference in precipitation, temperature, and atmospheric circulations. Rainfall, a useful climate indicator in the region, is distributed unequally in time and space. For instance, Fig. 2 presents the averaged daily precipitation for each of the climatic zones (Guinea coast, Savannah, and Sahel) during the wet and dry year composites. The seasonality of the monthly mean of daily rainfall shows regional variance, thereby highlighting the distinct spatial complexity of the WAM. Figure 2a, b shows the well-established two rainfall peaks, which is associated with the meridional migration of the Inter-Tropical Discontinuity (ITD) (Nicholson 2013, among others) and postulated "monsoon jump" (Sultan and Janicot 2000; Le Barbé et al. 2002), in the month of June and September over the Guinea coast. These peaks are observed for both wet and dry summer monsoon seasons in observations and model outputs. However, there is variance in magnitude, most especially, during the wet monsoon. In Savannah (Fig. 2c, d), a single peak is observed. The peak is observed in August (September) for wet (dry) monsoon year. The models reasonably agree in dry years unlike the wet years where only the WSM5-MYNN-nTDK simulates its peak in September. The more homogeneous Sahel zone shows a single peak in the month of August (Fig. 2e, f). The WSM5-MYNN-nTDK underestimates the observed precipitation in both monsoon composites while WSM5-YSU-nSAS overestimates the observed precipitation mostly in dry monsoon. However, all the model simulations show good agreement in the Sahel.

2.2 Monsoon simulation

The model was initialized in the month of February for each year of the four runs. Each run starts from February through to the end of October. Outputs in the initial month were however used as spin-up in all simulations. The current study analyzes

Table 2 The three different WRF model physics combinations derived from the selected schemes

| S/N	MP	PBL	CU
RUN 1	WSM5	MYNN	nTDK
RUN 2	GD	MYJ	BMJ
RUN 3	WSM5	YSU	nSAS

Fig. 1 Model domain and elevation used for the WRF simulations. The three climatic zones (**a** Guinean coast, **b** Savannah, and **c** Sahel) for area-averaged analysis are outlined on the map
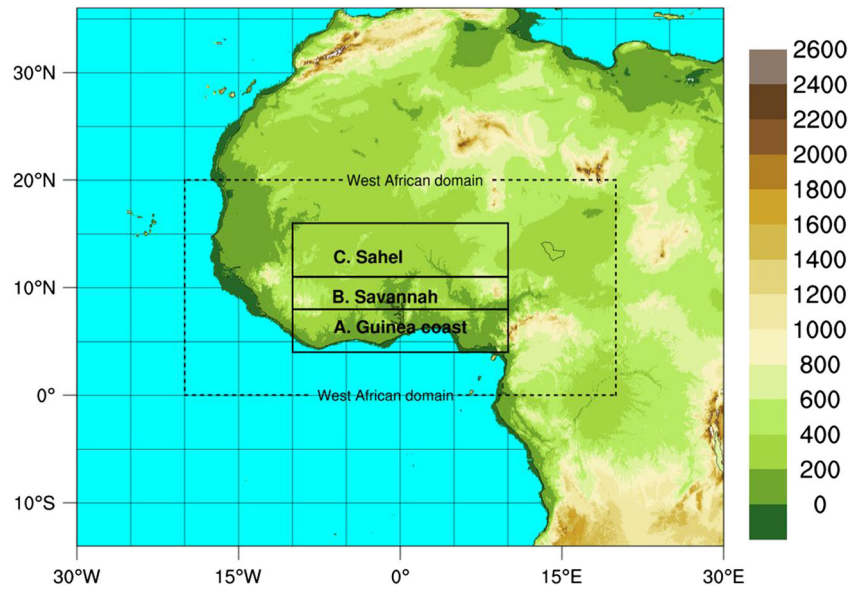
the months of June to September (JJAS) from the composites of wet (2008 and 2010) and dry (2001 and 2011) WAM years. These months were considered because this is the

period when the WAM is more active and most parts of West Africa receive a considerable amount of rainfall. Though the choice of the wet and dry years may not

Fig. 2 Seasonal cycle of area-averaged precipitation over the Guinean coast, Savannah, and Sahel climatic zones from the three experiments, TRMM and GPCP observation during wet (**a, c,** and **e**) and dry (**b, d,** and **f**) year's composite
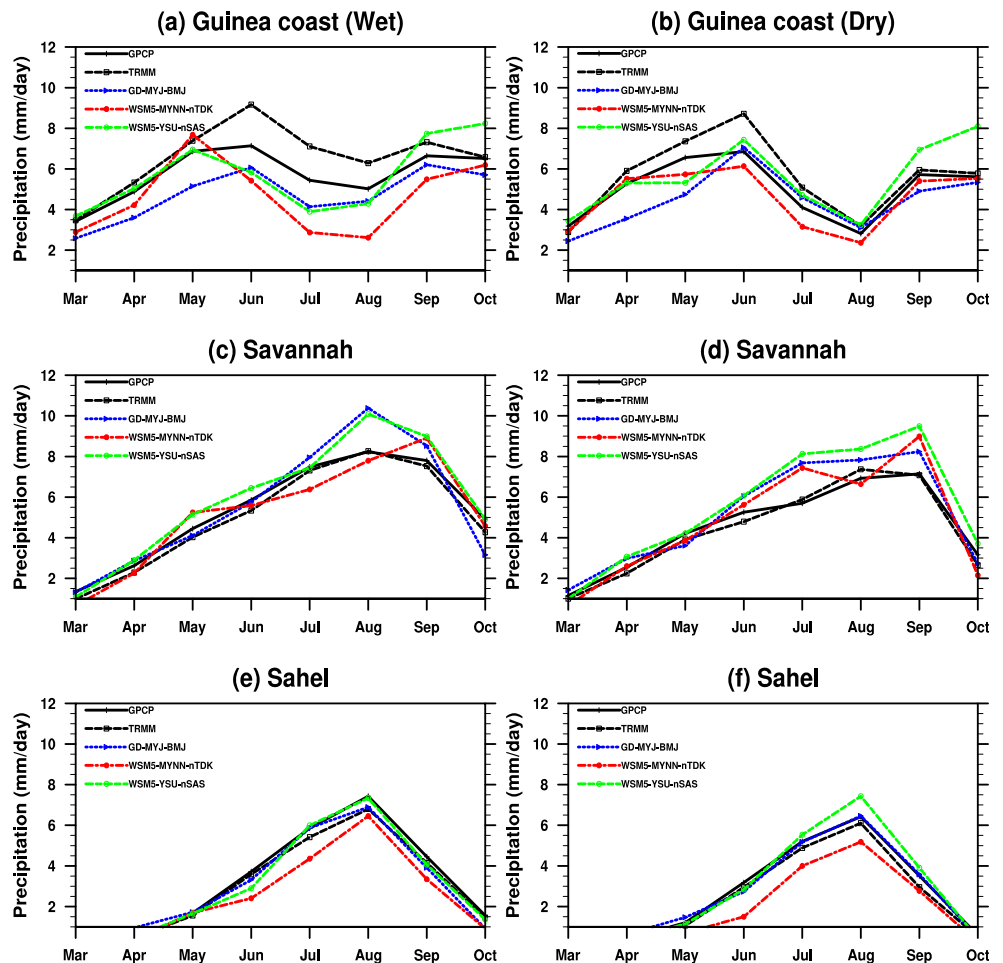
be all-encompassing to evaluate the performance of the WRF model to reproduce WAM variability, it gives useful insights. Some useful information that could be derived from the selected monsoon years to confirm the robustness in simulating WAM is on its associated precipitation and atmospheric circulation. The monsoon composites were used to assess the role of strong and weak circulations and moisture fluxes on the characteristics of WAM.

Composites of wet (2008 and 2010) and dry (2001 and 2011) monsoon years depict the characteristics of weak and strong atmospheric circulations and how these differences influence the WAM activity. Precipitation can be used to describe the observed differences in wet and dry years. Klein et al. (2015) used the Global Precipitation Climatology Center (GPCC) 0.5° gridded gauge analysis (Schneider et al. 2014) data to show that the selected years are categorized among wet and dry monsoon years. The grouping is based on the yearly precipitation departure from long-term mean over the study region.

2.3 Datasets

Model simulations are compared with reanalysis data and satellite observations in order to explain the behavior of the different monsoon composites produced from the selected model physics combinations. Data from the Global Precipitation Climatology Project (GPCP) 1° daily is used as reference to evaluate the model's precipitation. GPCP is a reliable satellite rainfall product obtained from merged estimates of microwave, infrared, and sounder data together with rainfall gauge analysis (Huffman et al. 2009, 2016). GPCP is used as reference rainfall because of its remarkable performance, and the product has been described to be the closest alternative source to station gauges over the West African region (Sylla et al. 2013). Another precipitation product used is the three hourly and 0.25° horizontal resolution 3B42 Tropical Rainfall Measurement Mission (TRMM) data, a reliable high-quality precipitation estimate from a satellite platform (Huffman et al. 2007).

Other model fields such as the moisture, temperature, and circulation are compared with the National Center for Environmental Prediction-Department of Energy (NCEP-DOE) Atmospheric Model Intercomparison Project (AMIP-II) reanalysis (R-2) datasets (NCEP-DOE AMIP R2, Kanamitsu et al. 2002, here after NCEP). The NCEP is available in 2.5° × 2.5° horizontal resolution at 17 vertical pressure levels. It consists of omega, zonal, and meridional winds, specific humidity, and temperature data among others. Though the difference in NCEP is much smaller from that in NCEP reanalysis 1 (Kalnay et al. 1996), it contains improvements through error fixes and parameterization updates (Kanamitsu et al. 2002).

3 Results and discussions

3.1 Rainfall

The rainfall climatology of wet and dry composites of the West African summer monsoon season is analyzed. Figure 3 depicts the spatial distribution of mean daily rainfall for the period June–September (JJAS) derived from the composites of wet and dry years for GPCP, TRMM, and the three model experiments as well as the model differences relative to GPCP. During JJAS, the spatial distribution of observed rainfall exhibits a meridional gradient with rainfall decreasing in intensity from the Guinea coast to the Sahel in association with the latitudinal migration of the ITD, which combines with the Saint Helena anticyclonic high pressure to control the monsoon wind that determines the amount of moisture influx into the region (Sultan and Janicot 2003). The observed localized maxima over the Jos Plateau, Cameroun Mountains and over the west coast of Guinea along 5°–10° N and Fouta-Djallon highlands are reproduced in the wet and dry year composites. Also, over this terrain, the observed rainfall amount is higher in the wet than the dry WAM season (Sultan and Janicot 2003; Im et al. 2014).

Although both wet and dry WAM composites show similar observed features, they exhibit some difference in terms of spatial magnitude. During wet WAM year, GD-MYJ-BMJ (bottom panel of Fig. 3a) overestimates rainfall between 1 and 5 mm day^{-1} offshore of west coast of Guinea, over the Fouta-Djallon and Cameroun Mountains. The same combination shows dry bias of about 3 mm day^{-1} in the western part of the region above 10° N and southern coast of Guinea along 5° N latitude. On the other hand, GD-MYJ-BMJ simulates increased wet bias above 4 mm day^{-1} and decreased dry bias below 3 mm day^{-1} in dry WAM season (bottom panel of Fig. 3b). The WSM5-MYNN-nTDK combination simulates extensive spatial coverage of dryness above 4 mm day^{-1} over the ocean and 2 mm day^{-1} or less in most parts of land areas in the wet WAM season. Also, the combination produces 3–5 mm day^{-1} wetness over the Fouta-Djallon, Jos Plateau, and Cameroun Mountains. The intensity of the dry (wet) biases decreased (increased) significantly during the dry (wet) WAM season mostly over the ocean. For the WSM5-YSU-nSAS combination, the model agrees well with the observed spatial pattern by producing much less dry bias of 3 mm day^{-1}, compared with other simulations, over some small spatial areas in both wet and dry WAM seasons, but it, however, overestimates by more than 3 mm day^{-1} over high terrain. Similar to the WSM5-MYNN-nTDK, the magnitude of the dryness (wetness) in the WSM5-YSU-nSAS simulation decreased (increased) during the dry (wet) WAM season. On average, WSM5-MYNN-nTDK simulations are relatively dry, GD-MYJ-BMJ are moderately wet and dry while WSM5-YSU-nSAS are comparatively wet with respect to GPCP.
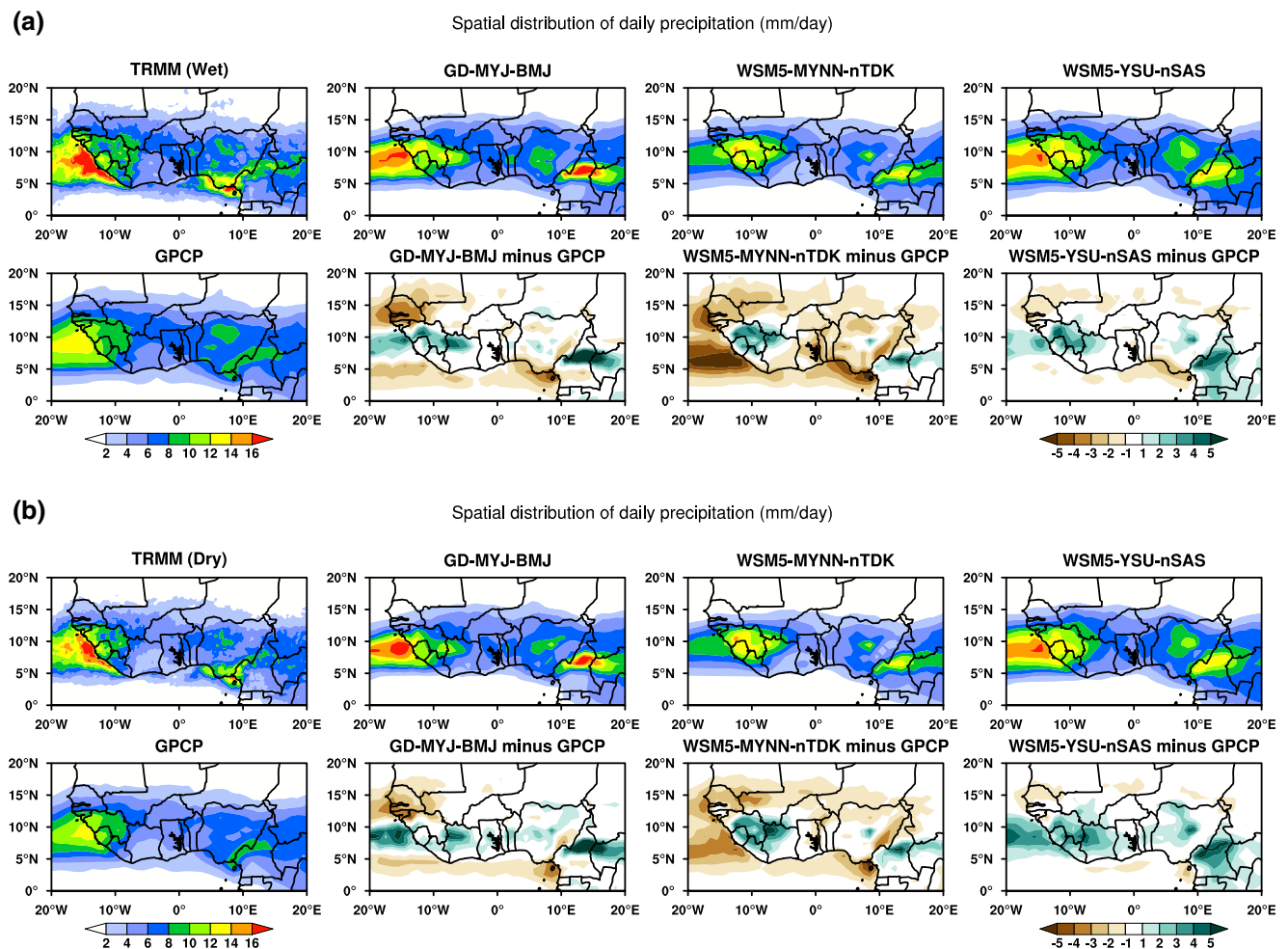
Fig. 3 Spatial distribution of mean **a** wet year (2008 and 2010) and **b** dry year (2001 and 2011) composite boreal summer (JJAS) precipitation (mm day^{-1}) from the TRMM and GPCP observations, three experiments, and their differences with GPCP observations

The common shortcoming in all simulations appears around the Cameroun Mountains, Jos Plateau, and over the Fouta-Djallon extending towards western coast of Guinea. All the three model combinations fail to accurately capture the intensity of the localized maximum over these high terrains regardless of the cloud microphysics, cumulus convection, and planetary boundary layer schemes used, thus showing significant dry and wet spatial biases. Such systematic biases displayed in the models are not limited to the simulations of the current study, but appears to be a quite typical error found in many other regional climate simulations over West Africa (Sylla et al. 2009; Flaounas et al. 2011; Zaroug et al. 2013; Im et al. 2014; Klutse et al. 2014; Klein et al. 2015; Gbode et al. 2018). Differences among the three model combinations can be explained by the difference in the physics used (Nikulin et al. 2012; Klein et al. 2015; Gbode et al. 2018). For instance, both GD-MYJ-BMJ and WSM5-MYNN-nTDK use a local closure PBL scheme, that is, MYJ and MYNN, where the eddy diffusion coefficients are derived from their prognostic turbulent kinetic energy (TKE). Contrarily, WSM5-YSU-

nSAS uses a non-local closure scheme with a parameter that allows enhanced vertical mixing and entrainment of air from above the PBL even in a neutral boundary layer where the vertical gradient of potential temperature is zero (Hong et al. 2006). This difference allows the combination with YSU PBL to possess enhanced deep convection and thus produce more spatial wetness relative to other combinations as a result of a stronger water cycle possibly due to increased evaporation associated with a more strongly mixed PBL, which serves as a source for consistent production of more vertical transport by convection into the troposphere (Ulate et al. 2014). Also, the profile adjustment convection scheme (BMJ) appears to produce less fraction of total rainfall (approximately 75% or less) compared with the mass flux nTDK and nSAS CU schemes (not shown), which can produce total rainfall fraction of 80% and above.

To further evaluate the model ability to reproduce different WAM seasons, the quantitative measure of rainfall produced in the model relative to observations is given in Table 3. Table 3 presents the total rainfall amount over the three

Table 3 Total rainfall (mm) for wet and dry monsoon seasons over the three climatic zones. The italic values indicate cases where wet years are consistent in both observations and models

Monsoon	Year	GPCP	TRMM	GD-MYJ-BMJ	WSM5-MYNN-nTDK	WSM5-YSU-nSAS
		Guinea coast				
Dry	2001	1291.2	1423.5	1069.1	1106.7	1326.0
	2011	1153.7	1311.5	1109.1	1132.2	1385.2
Wet	2008	*1421.6*	*1607.5*	*1136.9*	*1202.4*	*1436.1*
	2010	*1367.0*	*1592.3*	*1174.4*	1076.2	1340.7
		Savannah				
Dry	2001	1155.7	1121.0	1254.0	1135.4	1367.3
	2011	1049.7	1014.9	1224.1	1183.1	1324.8
Wet	2008	*1330.2*	*1260.4*	*1359.8*	*1281.1*	*1405.1*
	2010	*1276.6*	*1184.8*	*1336.4*	*1251.2*	*1461.1*
		Sahel				
Dry	2001	671.6	602.6	652.3	460.9	722.8
	2011	588.4	557.8	621.4	450.3	616.1
Wet	2008	*764.5*	*708.2*	*702.8*	*596.3*	671.0
	2010	*774.4*	*730.3*	*752.4*	*604.7*	*790.8*

different climatic zones; the italic values indicate cases where wet years are consistent in both observations and models. This was done to see how well the models are able to distinguish between wet and dry years. The skill of individual models to distinguish wet and dry years will give more confidence in its ability to show climate change signals in future work. Observed rainfall amounts agree quite well and are consistent for wet and dry years in GPCP and TRMM; however, the latter appears to have more rainfall on the Guinea coast where the differences are large. GD-MYJ-BMJ skillfully reproduced the selected wet and dry years in the three climatic zones, though with varying magnitudes. WSM5-MYNN-nTDK failed to reproduce one of the two wet years on the Guinea coast but was however skillful in distinguishing the different WAM seasons over Savannah and Sahel. In WSM5-YSU-nSAS, the model appears to have difficulty in differentiating wet and dry years in the Guinea coast and Sahel regions. The inabilities of some of the models to clearly differentiate the selected WAM seasons suggest that they are unable to reproduce the peak phase of some observed rainfall events (Gbode et al. 2018). This was also seen clearly in Fig. 2a where the June peak is missed.

One important atmospheric variable that can be used to explain the variability of the West African climate is the rainfall (Nicholson 1989; Hulme 1992). Rainfall in the region responds to the latitudinal evolution of the rain belt, defined by the mean surface position of the ITD, which is tightly coupled with the displacement of the Inter-Tropical Convergence Zone (ITCZ) over the western coast of West Africa. This interaction gives way to the abrupt northward migration and gradual southward retreat of the rainfall during the monsoon cycle (Sultan and Janicot 2000; Le Barbé et al.

2002; Lebel et al. 2003; Hagos and Cook 2007; Nikulin et al. 2012; Hernández-Díaz et al. 2013). GPCP, TRMM, and the three experiments are used to place and compare the composites of wet and dry monsoon in an interannual perspective. Time–latitude cross sections that display the evolution of the monthly rainfall, averaged between longitudes 10° W and 10° E, over West Africa for the monsoon composites, are presented in Fig. 4. The seasonal migration and retreat of the monsoon is non-linear as indicated by the northward monsoon jump of maximum rainfall.

From GPCP (Fig. 4a, f), the first major quasi-stationary monsoon core appears near 5° N in mid-May for wet and dry years, which corresponds to the onset of the monsoon along the Guinea coast, whereas TRMM (Fig. 4b, g) shows that the core near the same latitude extends further into June for both composites. All simulation combinations also simulate the core near 5° N but with a different magnitude in May during wet years. This result is consistent with previous findings that both the observations and simulations portray abrupt transitions for the monsoon onset, maximum, and retreat with differing intensities (Eltahir and Gong 1996; Sultan and Janicot 2000; Im et al. 2014; among others). In contrast, the models simulate the core near 5° N later in June for dry composite. The distribution in WSM5-MYNN-nTDK extends from April to June. The results of the models suggest that the monsoon onset is early(late) in wet(dry) monsoon years around the Guinea coast.

The second high-intensity rain belt jumps towards the Sahel region, and the maximum core is observed around 11° N in August, when the monsoon reaches its peak, with differing magnitudes for wet and dry years. In TRMM, the maximum core extends southwards from 11° N to around 9° N and
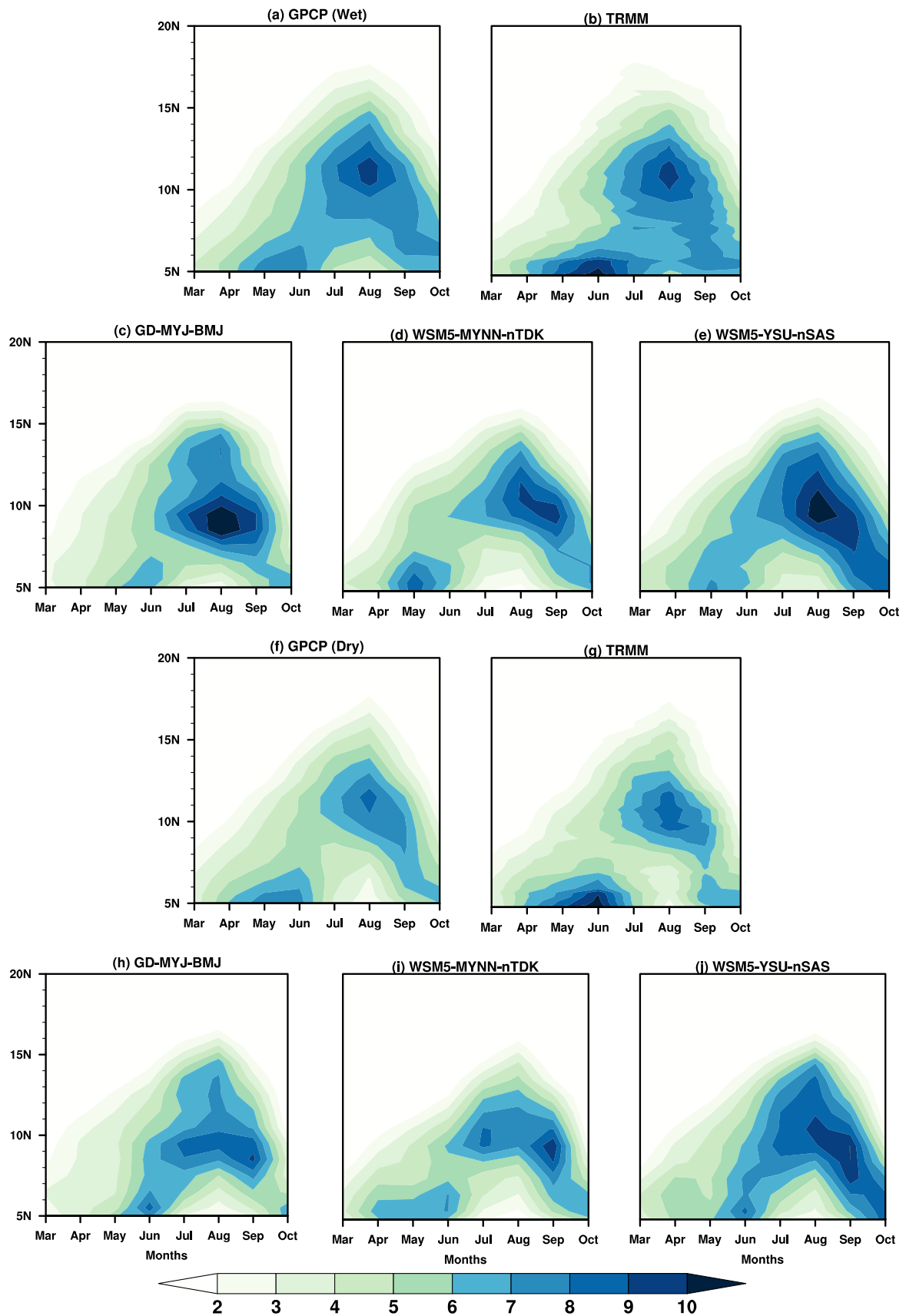
Fig. 4 Latitude–time cross section of monthly mean daily precipitation (mm day^{-1}) averaged from 10° W to 10° E from TRMM, GPCP observations, and the three experiments averaged over the **a**–**e** wet year (2008 and 2010) and **f**–**j** dry year (2001 and 2011) composites
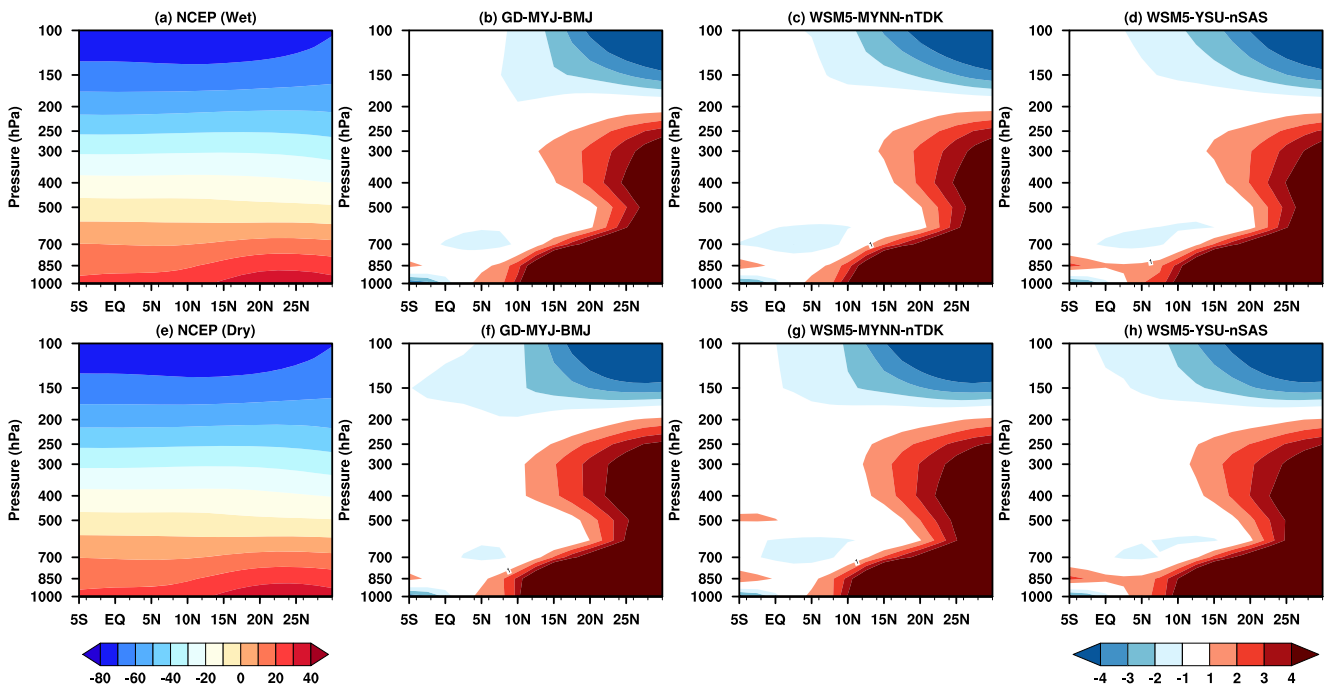
Fig. 5 Vertical cross section of JJAS mean temperature (°C) averaged over 10° W–10° E from NCEP, and the differences between the three experiments and NCEP for wet year (2008 and 2010) (top panels) and dry year (2001 and 2011) (bottom panels) composites

the rainfall amount in this phase is less than that in the first phase for both composites. Further, the monsoon retreats towards the Guinea coast around October, which marks the end of the season. During the wet years, all models simulate the maximum rainfall core between 9 and 10° N in August. In GD-MYJ-BMJ, the core is displaced southwards and that of WSM5-MYNN-nTDK extends to September. For dry year, the models maintain their mean latitudinal position but simulate an extended maximum rainfall core from July through to September. The core in September linearly extends southwards in WSM5-YSU-nSAS. Also, all simulations reproduce a noticeable core in September as well as southwards displacement of the rainfall core.

3.2 Vertical structure of temperature and humidity

The vertical cross section of zonal mean temperature averaged over 10° W and 10° E and the patterns of the model bias during the month of June through September (JJAS) for wet and dry year composites are presented in Fig. 5. A stratified region of maximum (minimum) temperature dominates the lower (upper) troposphere and a weak stratification at mid-layer. The core of the maximum temperature in the lower atmosphere around latitude 24° N corresponds to the Saharan heat low (SHL). This climatological feature appears in dry and wet years. SHL describes the existence of intense heating of the Sahara (Nicholson 2009; Thorncroft et al. 2011). Similarly, the two simulated monsoon composites reasonably replicate the vertical temperature gradient but with

varying magnitudes (not shown). A common characteristic of the models is an overestimation of temperature up to about 4 °C over land. This feature intensifies as it extends northwards from 5° N and around 11° N in the lower and mid-troposphere, respectively. This indicates a warm tropospheric bias over the Sahara Desert in the model regardless of the physics difference tested. Also, a compensating cold region resides in the upper atmosphere. These structures are clearly seen in the two composites, and they however possess wider coverage aside from their intensification in dry years.

Figure 6 depicts the vertical cross section of JJAS mean specific humidity averaged over longitudes 10° W–10° E and the differences between the three model experiments for wet and dry composites. Unlike temperature that is isothermal along latitudes, specific humidity decreases with increasing latitudes. In JJAS, the mean core of maximum humidity is situated at about latitude 10° N. This characteristic is peculiar in both wet and dry composites. All simulations underestimate (overestimate) atmospheric moisture over ocean (land) and Sahel region. This explains the overestimation of rainfall over the expected region of maxima and other areas of West Africa (as shown in Fig. 3). The models also overestimates the maximum at 10° N with other similar bias patterns over ocean and land areas for wet and dry composites. A warm bias over land areas can however enhance the excessive moisture that can lead to higher moist static energy, which could cause an increase in the convective available potential energy and thus create a favorable environment for induced convection (Eltahir 1998; Findell and Eltahir 2003).
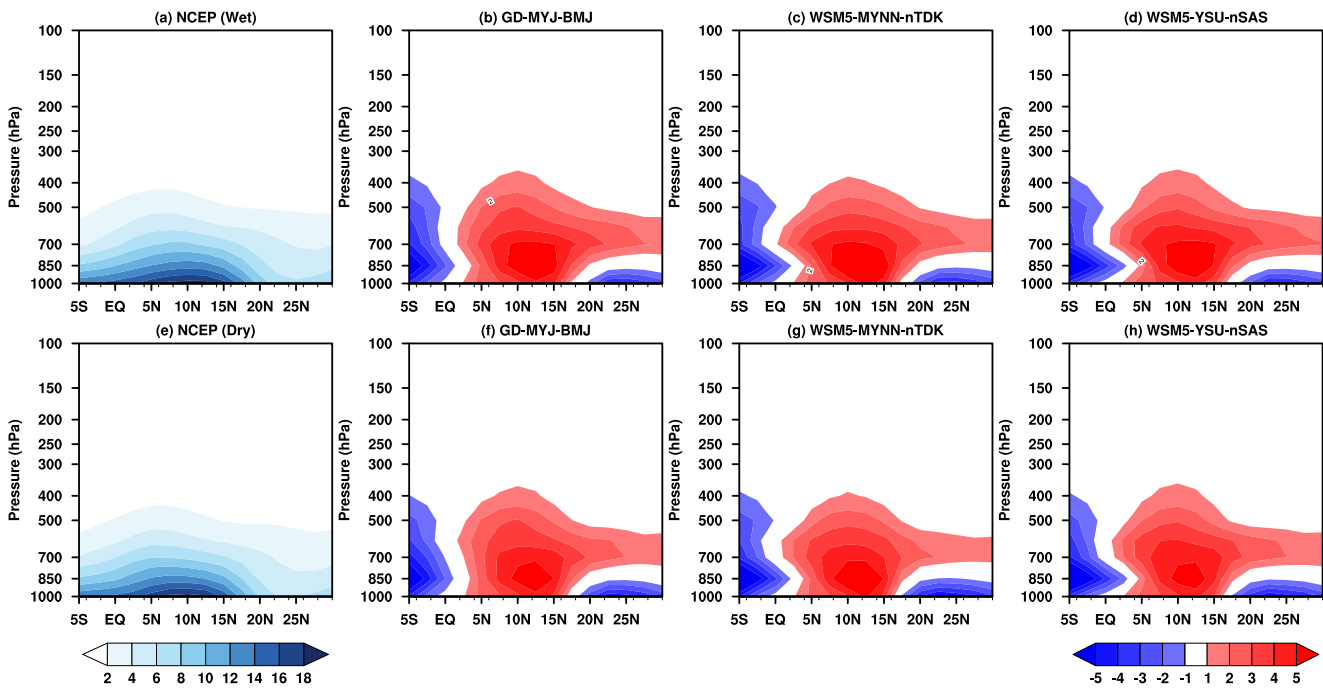
Fig. 6 Vertical cross section of JJAS mean specific humidity (g kg^{-1}) averaged over 10° W–10° E from NCEP, and the differences between the three experiments and NCEP for wet year (2008 and 2010) (top panels) and dry year (2001 and 2011) (bottom panels) composites

3.3 Large-scale circulation

The model performance with respect to the large-scale circulation is assessed at three levels to gain useful insight about the simulated three-dimensional dynamical structure of WAM system. Figure 7 displays wind vectors at 850, 650, and 150 hPa averaged for the month of August derived from the three simulations driven by ERA-Interim (and NCEP FNL soil only) as well as the NCEP reanalysis. In order to conserve the properties of dynamic fields and reduce excessive cancellation effects, only the results of August, which represents the peak of WAM activity, are provided for both wet and dry composites instead of the mean JJAS.

At low levels (850 hPa), the NCEP reanalysis shows that a westerly monsoon flow dominates the Guinea coast and Savannah zones. This flow transports moisture from the Atlantic Ocean into the region. North of 20° N, the winds are predominantly northeasterlies that carry dry and dusty air into the region. Where the two trade winds meet over land denotes the ITD position. The simulations all reproduce these observed features at low levels except for WSM5-MYNN-nTDK, which simulated stronger westerly monsoon flow in the wet season along the Guinea coast. In the wet WAM composite, WSM5-MYNN-nTDK and WSM5-YSU-nSAS simulations agree well with the observed monsoon flow, though WSM5-MYNN-nTDK simulates much stronger winds around the Cameroun Mountains. For GD-MYJ-BMJ, the wind magnitude is also high over the Cameroun Mountains

and the moisture influx is less due to easterlies along south coast, which weakens the monsoonal flow. Also, the GD-MYJ-BMJ and WSM5-MYNN-nTDK simulations reproduce the westerly monsoon flow further north. For the dry composite, there is a general increase in winds over Cameroun Mountains. GD-MYJ-BMJ simulates an anticyclonic flow over the southwestern coast of the region. Likewise, the moisture flux extends further inland in all simulations. The characteristics of the atmospheric circulation at this level are consistent with previous studies that reported observed maximum westerlies over the Cameroun Mountains and weak flow over the continent with longitudinal and latitudinal extents of 20° E and above 18° N, respectively (Akinsanola and Ogunjobi 2017).

At middle levels (650 hPa), strong easterly flow associated with the African Easterly Jet (AEJ) dominates (middle plots of Fig. 7). All simulations capture the major characteristics of the flow patterns at this level as they agree well with the observed maximum intensity and average location of maximum in NCEP. However, the simulations were unable to simulate the observed weak easterlies along the south coast of the region. During wet years, easterly winds are weaker which is necessary to allow more influx of moisture into the region that favors convective activity (Grist and Nicholson 2001; Dezfuli and Nicholson 2011). Though GD-MYJ-BMJ simulates stronger easterlies over the Guinea coast, it reproduces a better zonal band of AEJ. In WSM5-MYNN-nTDK and WSM5-YSU-nSAS, the intensity of the AEJ belt decreases
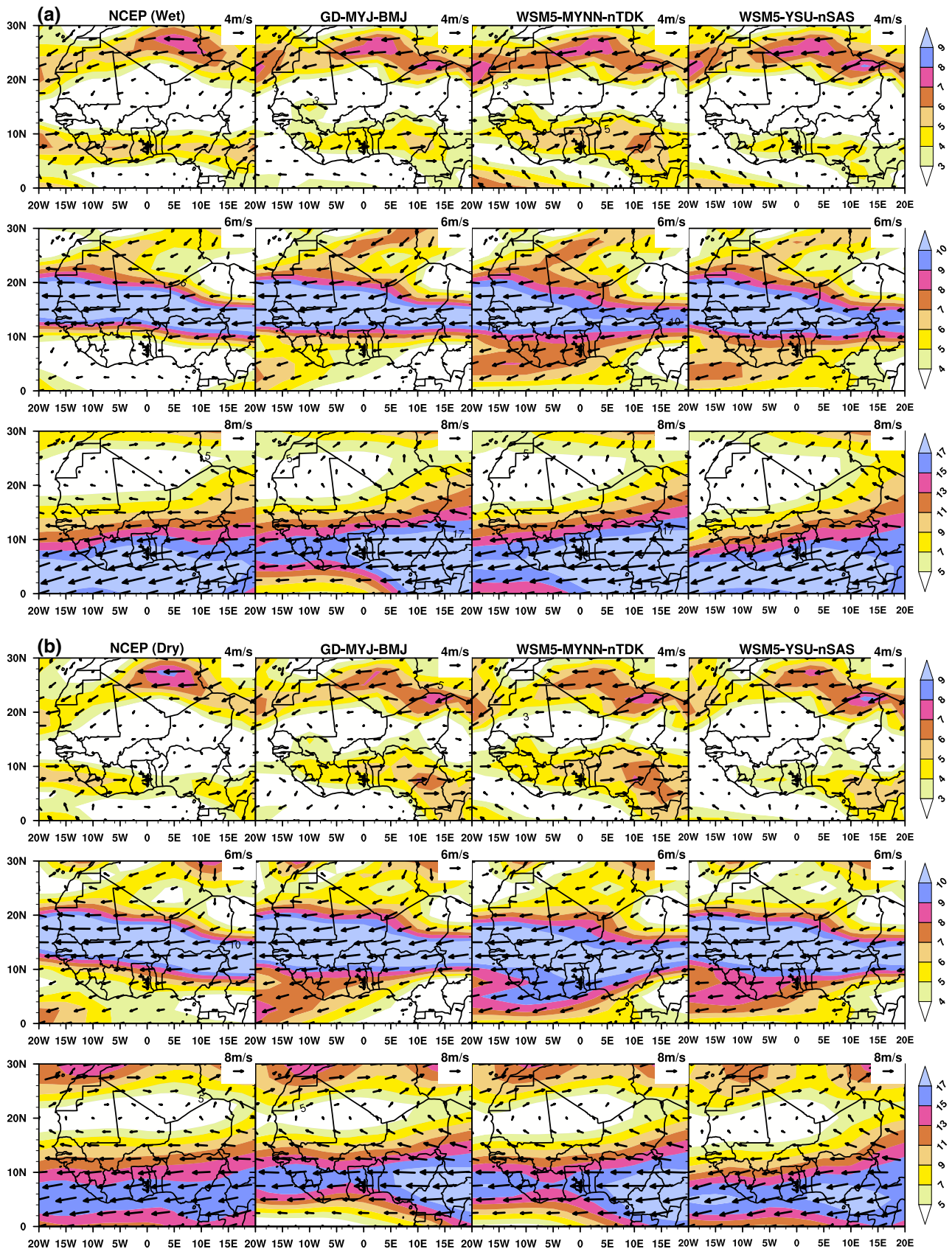
Fig. 7 Spatial distribution of wind vectors at 850 (top), 650 (middle), and 150 hPa (bottom) averaged for the month of August from the three simulations and NCEP. Here, color shading indicates the speed of the wind (m s^{-1}) for **(a)** wet year (2008 and 2010) and **(b)** dry year (2001 and 2011) composites
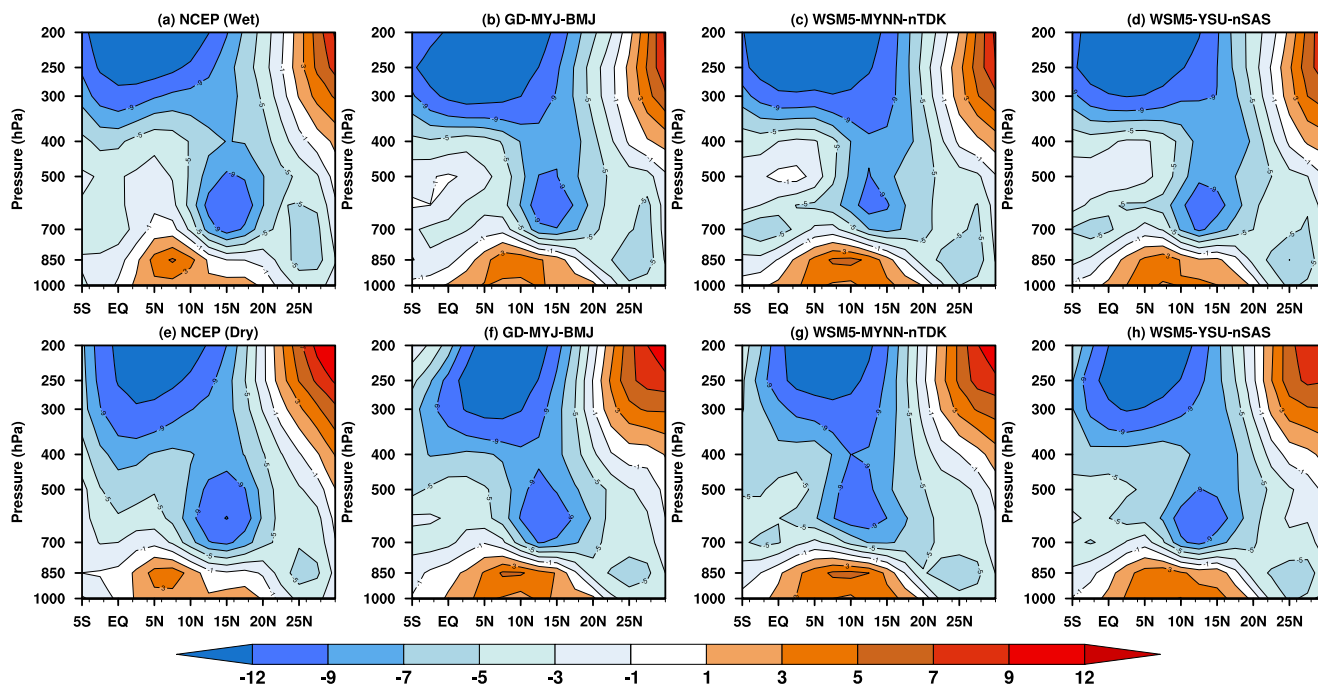
Fig. 8 Vertical cross section of zonal wind (m s^{-1}) averaged from longitude 10° W to 10° E for the month of August from NCEP and the three experiments for wet year (2008 and 2010) (top panels) and dry year (2001 and 2011) (bottom panels) composites

eastward. For dry years, the observed and modeled AEJ intensifies and there is a noticeable increase in coastal easterlies. The meridional extent of the AEJ belt increases in all simulations. WSM5-MYNN-nTDK exhibits the strongest winds and extends southwards to the coast of the region. This causes the depth of the low-level moisture flux to decrease and in turn bring about a reduction in rainfall amount (Fig. 3).

Finally, at upper levels (150 hPa), there is a strong wide zonal band of easterlies associated with the Tropical Easterly Jet (TEJ), which is caused as a result of mass outflow around the Himalayas. This zonal band of easterlies extends across the Guinea region. Also, noticeable are westerly winds north of the WAM domain. The strong upper tropospheric flows and the resultant divergence are consistent with the simulated low-level convergence, which enhance rising motion of moist and warm air from near the surface (see Fig. 9). The simulations are able to reproduce these two major observed features of the upper-level flow. Further, the simulations reproduce the observed TEJ intensification during the wet year and weakening in the dry year. This suggests that the model is able to allow the mass outflow from the Himalayas to propagate into the southeastern corner of the model domain but, however, at higher magnitudes most especially in dry years. The TEJ is described to play a role in the development of the rainbelt over West Africa (Nicholson and Grist 2003; Nicholson 2009).

Figure 8 depicts the vertical structure of the zonal wind averaged from 10° W and 10° E longitudes for the month of August. The vertical structure portrays the stratified behavior

of the atmospheric circulation with three major components that are consistent with the results of Akinsanola et al. (2015) among others. The prevailing westerly flow up to 850 hPa describes the monsoon flow, and the two easterly maxima centered on 650 hPa and 200 hPa describe the AEJ and TEJ, respectively. The westerly monsoon flow dominates between the equator and beyond 15° N. The position and intensity of the monsoon flow is an important factor that determines the magnitude and spatial distribution of rainfall in the region. From NCEP, the depth of the monsoon extends further upwards and its core shifts northward in wet year contrary to the dry year where it is less deep. All simulations reproduce this characteristic but with a broader zonal extent. However, the strength of the simulated monsoon flow for both composites is comparable with the reanalysis.

The AEJ is a paramount feature of the WAM dynamics, and it is associated with strong baroclinic atmospheric conditions caused by the strong meridional surface temperature gradient and moisture between the Sahara and equatorial Africa (Newell and Kidson 1984; Cook 1999; Thorncroft and Blackburn 1999; Thorncroft et al. 2003). All simulations reasonably reproduce the mean position of the AEJ centered on 650 hPa for wet and dry composites. Also, all the simulations reproduced intensified AEJ in dry year as well as shift of the jet core southwards from the average latitudinal position of 15° N.

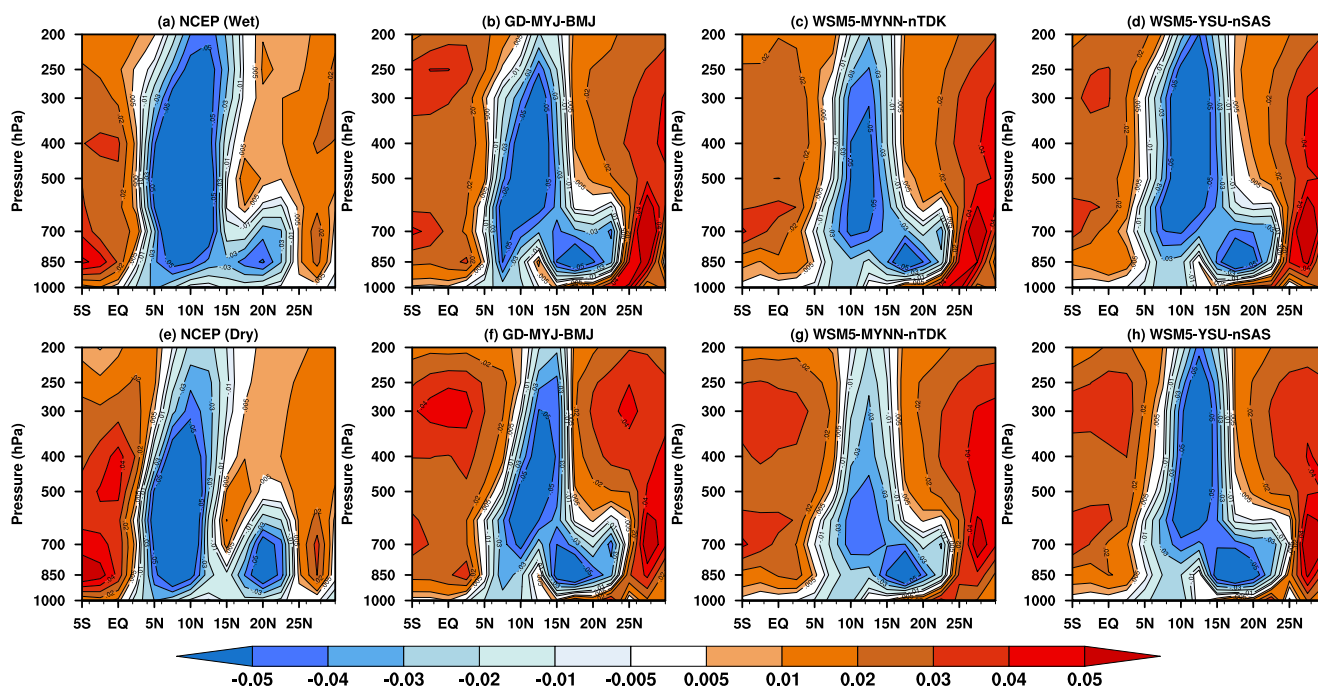Considering the TEJ, all simulations reasonably reproduce the strength, depth, and latitudinal position compared with

Fig. 9 Vertical cross section of omega (Pa s^{-1}) averaged from longitude 10° W to 10° E for the month of August from NCEP and the three experiments for wet year (2008 and 2010) (top panels) and dry year (2001 and 2011) (bottom panels) composites

NCEP composites. The models also simulate the downward extension of the jet core in a dry year.

Figure 9 presents the vertical cross section of mean vertical motion averaged along longitudes 10° W and 10° E in the month of August. The figure clearly defines the described two regions of vertical ascent (Nicholson 2009). The first region of ascent (blue) lies between the mean latitudinal position of AEJ (~15° N) and TEJ (~5° N), while the second shallow region of vertical ascent resides around the surface position of the ITD and center of the Saharan heat low. The vertical ascent shows strong sensitivity to the choice of physics options, most especially the PBL and convection schemes as found in preliminary study (Gbode et al. 2018). Irrespective of the disparities in the simulated shape and magnitude, two locations of strong ascending motion are reproduced in the wet and dry year simulations when compared with reanalysis. The depth of the major region of ascent extends beyond 200 hPa with its core positioned around 10° N. This region is related to convective activity, and it corresponds to the latitudinal position of maximum rainfall amount (Nicholson 2009). All simulations are able to reproduce this ascent but with different meridional width. However, the structure of WSM5-YSU-nSAS appears to agree well with the reanalysis. During wet years, when the ascent is strongest, the meridional width broadens and shifts slightly northwards. In a dry year, when the ascent is usually weak, it is narrow with a southward displacement and its core extends to about 300 hPa. WSM5-MYNN-nTDK has a more shallow southern extension of ascent core, which makes it underestimate rainfall most

especially within the zonal band of 5° N to 10° N (see Fig. 3). While the WSM5-MYNN-nTDK simulation shows underestimates, WSM5-YSU-nSAS overestimates the rainfall distribution. The ascending motion is strongest in WSM5-YSU-nSAS, followed by GD-MYJ-BMJ and WSM5-MYNN-nTDK during wet and dry years. Its strength is more in WSM5-YSU-nSAS in the dry years. This result strongly impacts the simulated rainfall amount and distribution, that is, consistent with the overestimated rainfall in WSM5-YSU-nSAS, moderate distribution in GD-MYJ-BMJ, and underestimation in WSM5-MYNN-nTDK. This impact is clearly seen over the west coast of the region. However, there is a need to extend the present study by performing more detailed dynamic investigation in future work so as to further understand the underlying mechanisms responsible for the observed monsoon jump.

4 Conclusion

This paper presents results of simulations of wet and dry WAM years using the WRF regional climate model. Three different physics combinations of microphysics, cumulus convection, and planetary boundary layer schemes were considered. Other schemes like the unified Noah land-surface model scheme and RRTMG schemes were used to represent the land surface and radiation processes, respectively. The model was run for four WAM seasons that consist of two wet (2008 and 2010) and two dry years (2001 and 2011). The four

simulations were used to compute composites of wet and dry WAM seasons.

The results presented here depict that simulation of the WAM showed strong sensitivity to the choice of both the planetary boundary layer and the convection scheme. One of the good agreements with observations in the simulation of the WAM rainfall distribution pattern was with WSM5-YSU-nSAS because it was able to reproduce better circulation features that are associated with typical wet and dry WAM. However, the combination was unable to quantitatively differentiate between wet and dry years as compared with GD-MYJ-BMJ and WSM5-MYNN-nTDK, which produced both a good seasonal evolution and magnitude of the monsoon rainfall. On the contrary, WSM5-MYNN-nTDK tends to underestimate rainfall along the coast especially over the western coast of West Africa and the tropical Atlantic Ocean. Simulation outputs from GD-MYJ-BMJ show moderate spatial overestimates and underestimates of rainfall compared with the GPCP product over the region. The inconsistent simulation of the observed circulation features related to the WAM activity caused the WSM5-MYNN-nTDK to perform less well with respect to observed rainfall. However, this combination and others were able to reproduce good vertical distributions of temperature and moisture profiles, though with warm and wet biases over land and the reverse over the ocean region. This feature is noticeable during the wet and dry WAM seasons.

Lastly, it was shown that the WRF regional climate model is capable of reproducing the main features of the large-scale circulation during wet and dry WAM periods. During these periods, the three model experiments were able to capture the low-level westerly monsoon flow, middle-level African easterly jet, and upper tropospheric tropical easterly jet. Also, two of the model combinations, GD-MYJ-BMJ and WSM5-MYNN-nTDK, demonstrate a significant skill in capturing the difference in wet and dry WAM seasons as shown in this study. The outcomes presented here suggest a significant potential for WRF model as a useful tool to investigate how future WAM seasons could vary with climate change in order to understand the possible implications of such variability on economic activities such as agriculture, water resources, and other climate-related sectors of the economy.

References

Abiodun BJ, Salami AT, Matthew OJ, Odedokun S (2013) Potential impacts of afforestation on climate change and extreme events in Nigeria. Clim Dyn 41(2):277–293. https://doi.org/10.1007/s00382-012-1523-9

Afiesimama EA, Pal JS, Abiodun BJ, Gutowski WJ, Adedoyin A (2006) Simulation of West African monsoon using the RegCM3. Part I: model validation and interannual variability. Theor Appl Climatol 86(1–4):23–37

Akinsanola AA, Ogunjobi KO, Gbode IE, Ajayi VO (2015) Assessing the capabilities of three regional climate models over CORDEX Africa in simulating west African summer monsoon precipitation. Adv Meteorol 2015, Article ID 935431, https://doi.org/10.1155/2015/935431

Akinsanola AA, Ogunjobi KO (2017) Evaluation of present-day rainfall simulations over West Africa in CORDEX regional climate models. Environ Earth Sci 76:366. https://doi.org/10.1007/s12665-017-6691-9

Akinsanola AA, Ajayi VO, Adejare AT, Adeyeri OE, Gbode IE, Ogunjobi KO, Nikulin G, Abolude AT (2018) Evaluation of rainfall simulations over West Africa in dynamically downscaled CMIP5 global circulation models. Theor Appl Climatol 132(1–2):437–450

Akinsanola AA, Zhou W (2018) Dynamic and thermodynamic factors controlling increasing summer monsoon rainfall over the West African Sahel. Clim Dyn 52:4501–4514. https://doi.org/10.1007/s00382-018-4394-x

Baines PG, Folland CK (2007) Evidence for rapid global climate shift across the late 1960s. J Clim 20:2721–2744. https://doi.org/10.1175/JCLI4177.1

Burpee RW (1972) The origin and structure of easterly waves in the lower troposphere in North Africa. J Atmos Sci 29:77–90

Charney JG, Quirk WJ, Chow SH, Korn eld J (1977) A compara- tive study of the e ects of albedo change on drought in semi-arid regions. J Atmos Sci 34:1366–1385

Chen F, Dudhia J (2001) Coupling an advanced land surface–hydrology model with the Penn State–NCAR MM5 modeling system. Part I: model implementation and sensitivity. Mon Weather Rev 129(4):569–585

Christensen JH, Hewitson B, Busuioc A, Chen A, Gao X, Held I, Jones R, Kolli RK, Kwon WT, Laprise R, Rueda VM, Mearns L, Menéndez CG, Räisänen J, Rinke A, Sarr A, Whetton P (2007) Regional climate projections, in: climate change: the physical science basis. Contribution of working group I to the fourth assessment report of the inter-governmental panel on climate change. In: Solomon S, Qin D, Manning M, Chen Z, Marquis M, Averyt KB, Tig-nor M, Miller HL, Cambridge University Press, Cambridge

Cook KH (1999) Generation of the African easterly jet and its role in determining West African precipitation. J Clim 12(5):1165–1184

Dee DP, Uppala SM, Simmons AJ, Berrisford P, Poli P, Kobayashi S, Andrae U, Balmaseda MA, Balsamo G, Bauer DP, Bechtold P (2011) The ERA-interim reanalysis: configuration and performance of the data assimilation system. Q J Roy Meteor Soc 137(656):553–597

Dezfuli AK, Nicholson SE (2011) A note on long-term variations of the African easterly jet. Int J Climatol 31(13):2049–2054

Eltahir EA, Gong C (1996) Dynamics of wet and dry years in West Africa. J Clim 9(5):1030–1042

Eltahir EA (1998) A soil moisture–rainfall feedback mechanism: 1. Theory and observations. Water Resour Res 34(4):765–776

Findell KL, Eltahir EA (2003) Atmospheric controls on soil moisture–boundary layer interactions. Part I: framework development. J Hydrometeorol 4(3):552–569

Flaounas E, Bastin S, Janicot S (2011) Regional climate modelling of the 2006 West African monsoon: sensitivity to convection and planetary boundary layer parameterisation using WRF. Clim Dyn 36(5–6):1083–1105

Gallée H, Moufouma-Okia W, Bechtold P, Brasseur O, Dupays I, Marbaix P, Messager C, Ramel R, Lebel T (2004) A high-resolution simulation of a West African rainy season using a regional climate model. J Geophys Res Atmos 109(D5)

Gbode IE, Dudhia J, Ogunjobi KO, Ajayi VO (2018) Sensitivity of different physics schemes in the WRF model during a West African monsoon regime. Theor Appl Climatol 136:1–19. https://doi.org/10.1007/s00704-018-2538-x

Grist JP, Nicholson SE (2001) A study of the dynamic factors influencing the rainfall variability in the West African Sahel. J Clim 14(7):1337–1359

Hagos SM, Cook KH (2007) Dynamics of the West African monsoon jump. J Clim 20(21):5264–5284

Hagos S, Leung LR, Xue Y, Boone A, de Sales F, Neupane N, Huang M, Yoon JH (2014) Assessment of uncertainties in the response of the African monsoon precipitation to land use change simulated by a regional model. Clim Dyn 43(9–10):2765–2775

Han J, Pan HL (2011) Revision of convection and vertical diffusion schemes in the NCEP global forecast system. Weather Forecast 26(4):520–533

Hernández-Díaz L, Laprise R, Sushama L, Martynov A, Winger K, Dugas B (2013) Climate simulation over CORDEX Africa domain using the fifth-generation Canadian Regional Climate Model (CRCM5). Clim Dyn 40(5–6):1415–1433

Hong SY, Dudhia J, Chen SH (2004) A revised approach to ice microphysical processes for the bulk parameterization of clouds and precipitation. Mon Weather Rev 132(1):103–120

Hong SY, Noh Y, Dudhia J (2006) A new vertical diffusion package with an explicit treatment of entrainment processes. Mon Weather Rev 134(9):2318–2341

Huffman GJ, Bolvin DT, Nelkin EJ, Wolff DB, Adler RF, Gu G, Hong Y, Bowman KP, Stocker EF (2007) The TRMM multisatellite precipitation analysis (TMPA): quasi-global, multiyear, combined-sensor precipitation estimates at fine scales. J Hydrometeorol 8(1):38–55

Huffman GJ, Adler RF, Bolvin DT, Gu G (2009) Improving the global precipitation record: GPCP version 2.1. Geophys Res Lett 36(17). https://doi.org/10.1029/2009GL040000

Huffman GJ, Bolvin DT, Adler RF (2016) GPCP version 1.2 one-degree daily precipitation data set. Research data archive at the National Center for Atmospheric Research, computational and information systems laboratory. doi:https://doi.org/10.5065/D6D50K46

Hulme M (1992) Rainfall changes in Africa: 1931–1960 to 1961–1990. Int J Climatol 12(7):685–699

Iacono MJ, Delamere JS, Mlawer EJ, Shephard MW, Clough SA, Collins WD (2008) Radiative forcing by long-lived greenhouse gases: calculations with the AER radiative transfer models. J Geophys Res Atmos 113(D13)

Iloeje NP (1981) A new geography of Nigeria. Longman, UK

Im ES, Gianotti RL, Eltahir EA (2014) Improving the simulation of the West African monsoon using the MIT regional climate model. J Clim 27(6):2209–2229

IPCC (2001) Climate Change 2001: The Scientific Basis. Contribution of Working Group I to the Third Assessment Report of the Intergovernmental Panel on Climate Change. In: Houghton JT, Ding Y, Griggs DJ, Noquer M, van der Linden PJ, Dai X, Maskell K, Johnson CA (eds) . Cambridge University Press, Cambridge, United Kingdom and New York, NY, USA, p 881

IPCC (2007) Climate Change 2007: The Physical Science Basis. Contribution of Working Group I to the Fourth Assessment Report of the Intergovernmental Panel on Climate Change. In: Solomon S, Qin D, Manning M, Chen Z, Marquis M, Averyt KB, Tignor M, Miller HL (eds) . Cambridge University Press, Cambridge, United Kingdom and New York, NY, USA, p 996

Janjić ZI (1994) The step-mountain eta coordinate model: further developments of the convection, viscous sublayer, and turbulence closure schemes. Mon Weather Rev 122(5):927–945

Janjić ZI (2000) Comments on "development and evaluation of a convection scheme for use in climate models". J Atmos Sci 57(21):3686–3686

Jones PW (1999) First-and second-order conservative remapping schemes for grids in spherical coordinates. Mon Weather Rev 127(9):2204–2210

Hoegh-Guldberg O, Jacob D, Taylor M, Bindi M, Brown S, Camilloni I, Diedhiou A, Djalante R, Ebi KL, Engelbrecht F, Guiot J, Hijioka Y, Mehrotra S, Payne A, Seneviratne SI, Thomas A, Warren R, Zhou G (2018) Impacts of 1.5 °C Global Warming on Natural and Human Systems. In: Global Warming of 1.5 °C. An IPCC Special Report on the impacts of global warming of 1.5 °C above pre-industrial levels and related global greenhouse gas emission pathways, in the context of strengthening the global response to the threat of climate change, sustainable development, and efforts to eradicate poverty. In: Masson-Delmotte, V. P. Zhai, H.-O. Pörtner, D. Roberts, J. Skea, P.R. Shukla, A. Pirani, W. Moufouma-Okia, C. Péan, R. Pidcock, S. Connors, J.B.R. Matthews, Y. Chen, X. Zhou, M.I. Gomis, E. Lonnoy, T. Maycock, M. Tignor, and T. Waterfield (eds). In Press

Kalnay E, Kanamitsu M, Kistler R, Collins W, Deaven D, Gandin L, Iredell M, Saha S, White G, Woollen J, Zhu Y (1996) The NCEP/NCAR 40-year reanalysis project. BAMS 77(3):437–472

Kanamitsu M, Kumar A, Juang HMH, Schemm JK, Wang W, Yang F, Hong SY, Peng P, Chen W, Moorthi S, Ji M (2002b) NCEP dynamical seasonal forecast system 2000. BAMS 83(7):1019–1038

Klein C, Heinzeller D, Bliefernicht J, Kunstmann H (2015) Variability of West African monsoon patterns generated by a WRF multi-physics ensemble. Clim Dyn 45(9–10):2733–2755

Klutse NAB, Sylla MB, Diallo I, Sarr A, Dosio A, Diedhiou A, Kamga A, Lamptey B, Ali A, Gbobaniyi EO, Owusu K, Lennard C, Hewitson B, Nikulin G, Panitz HJ, Büchner M (2014) Daily characteristics of West African summer monsoon precipitation in CORDEX simulations. Theor Appl Climatol 123:369–386. https://doi.org/10.1007/s00704-014-1352-3

Le Barbé L, Lebel T, Tapsoba D (2002) Rainfall variability in West Africa during the years 1950–90. J Clim 15(2):187–202

Lebel T, Diedhiou A, Laurent H (2003) Seasonal cycle and interannual variability of the Sahelian rainfall at hydrological scales. J Geophys Res Atmos, 108(D8)

Li R, Jin J, Wang SY, Gillies RR (2015) Significant impacts of radiation physics in the weather research and forecasting model on the precipitation and dynamics of the West African monsoon. Clim Dyn 44(5–6):1583–1594

Kanamitsu M, Ebisuzaki W, Woollen J, Yang S-K, Hnilo JJ, Fiorino M, Potter GL (2002) National Center for Environmental Predictions-Department of Energy (NCEP-DOE) Atmospheric Model Intercomparison Project (AMIP-II) Reanalysis-2. BAMS 11:1631–1643

Nakanishi M, Niino H (2004) An improved Mellor–Yamada level-3 model with condensation physics: its design and verification. Bound-Layer Meteorol 112(1):1–31

Nakanishi M, Niino H (2006) An improved Mellor–Yamada level-3 model: its numerical stability and application to a regional prediction of advection fog. Bound-Layer Meteorol 119(2):397–407

NCEP FNL (2000) National Centers for Environmental Prediction/ National Weather Service/ NOAA/U.S. Department of Commerce (2000) updated daily. NCEP FNL Operational Model Global Tropospheric Analyses, continuing from July 1999. Research Data Archive at the National Center for Atmospheric Research, Computational and Information Systems Laboratory. https://doi.org/10.5065/D6M043C6. Accessed 09 March 2017

Newell RE, Kidson JW (1984) African mean wind changes between Sahelian wet and dry periods. J Climatol 4(1):27–33

Nicholson SE (1989) Long-term changes in African rainfall. Weather 44(2):46–56

Nicholson SE, Grist JP (2003) The seasonal evolution of the atmospheric circulation over West Africa and equatorial Africa. J Clim 16(7): 1013–1030

Nicholson SE (2009) A revised picture of the structure of the "monsoon" and land ITCZ over West Africa. Clim Dyn 32(7–8):1155–1171

Nicholson SE (2013) The West African Sahel: a review of recent studies on the rainfall regime and its interannual variability. ISRN Meteor 2013. https://doi.org/10.1155/2013/453521

Nikulin G, Jones C, Giorgi F, Asrar G, Büchner M, Cerezo-Mota R, Christensen OB, Déqué M, Fernandez J, Hänsler A, van Meijgaard E (2012) Precipitation climatology in an ensemble of CORDEX-Africa regional climate simulations. J Clim 25(18): 6057–6078

Noble E, Druyan LM, Fulakeza M (2014) The sensitivity of WRF daily summertime simulations over West Africa to alternative parameterizations. Part I: African wave circulation. Mon Weather Rev 142(4): 1588–1608

Noble E, Druyan LM, Fulakeza M (2017) The sensitivity of WRF daily summertime simulations over West Africa to alternative parameterizations. Part II: precipitation. Mon Weather Rev 145(1):215–233

Omotosho JB, Abiodun BJ (2007) A numerical study of moisture build-up and rainfall over West Africa. Meteorol Appl 14(3):209–225. https://doi.org/10.1002/met.11

Prein AF, Gobiet A, Suklitsch M, Truhetz H, Awan NK, Keuler K, Georgievski G (2013) Added value of convection permitting seasonal simulations. Clim Dyn 41:2655–2677

Schneider U, Becker A, Finger P, Meyer-Christoffer A, Ziese M, Rudolf B (2014) GPCC's new land surface precipitation climatology based on quality-controlled in situ data and its role in quantifying the global water cycle. Theor Appl Climatol 115(1–2):15–40

Sultan B, Janicot S (2000) Abrupt shift of the ITCZ over West Africa and intraseasonal variability. Geophys Res Lett 27(20):3353–3356

Sultan B, Janicot S (2003) The West African monsoon dynamics. Part II: the "preonset" and "onset" of the summer monsoon. J Clim 16(21): 3407–3427

Sylla MB, Gaye AT, Pal JS, Jenkins GS, Bi XQ (2009) High-resolution simulations of West African climate using regional climate model (RegCM3) with different lateral boundary conditions. Theor Appl Climatol 98(3–4):293–314

Sylla MB, Coppola E, Mariotti L, Giorgi F, Ruti PM, Dell'Aquila A, Bi X (2010a) Multiyear simulation of the African climate using a regional climate model (RegCM3) with the high resolution ERA-Interim reanalysis. Clim Dyn 35:231–247. https://doi.org/10.1007/s00382-009-0613-9

Sylla MB, Dell'Aquila A, Ruti PM, Giorgi F (2010b) Simulation of the intraseasonal and the interannual variability of rainfall over West Africa with RegCM3 during the monsoon period. Int J Climatol 30:1865–1883. https://doi.org/10.1002/joc.2029

Sylla MB, Giorgi F, Coppola E, Mariotti L (2013) Uncertainties in daily rainfall over Africa: assessment of gridded observation products and evaluation of a regional climate model simulation. Int J Climatol 33(7):1805–1817. https://doi.org/10.1002/joc.3551

Tao WK, Simpson J, McCumber M (1989) An ice-water saturation adjustment. Mon Weather Rev 117(1):231–235

Tiedtke MICHAEL (1989) A comprehensive mass flux scheme for cumulus parameterization in large-scale models. Mon Weather Rev 117(8):1779–1800

Thorncroft CD, Blackburn M (1999) Maintenance of the African easterly jet. Q J Roy Meteor Soc 125(555):763–786

Thorncroft CD, Parker DJ, Burton RR, Diop M, Ayers JH, Barjat H, Devereau S, Diongue A, Dumelow R, Kindred DR, Price NM (2003) The JET2000 project: aircraft observations of the African easterly jet and African easterly waves: aircraft observations of the African easterly jet and African easterly waves. BAMS 84(3):337–352

Thorncroft CD, Nguyen H, Zhang C, Peyrillé P (2011) Annual cycle of the West African monsoon: regional circulations and associated water vapour transport. Q J Roy Meteor Soc 137(654):129–147

Ulate M, Dudhia J, Zhang C (2014) Sensitivity of the water cycle over the Indian Ocean and maritime continent to parameterized physics in a regional model. J Adv Model Earth Sys 6:1095–1120. https://doi.org/10.1002/2014MS000313

Xue Y, De Sales F, Lau WM, Boone A, Feng J, Dirmeyer P, Guo Z, Kim KM, Kitoh A, Kumar V, Poccard-Leclercq I (2010) Intercomparison and analyses of the climatology of the West African monsoon in the West African Monsoon Modeling and Evaluation project (WAMME) first model intercomparison experiment. Clim Dyn 35(1):3–27

Zaroug MA, Sylla MB, Giorgi F, Eltahir EA, Aggarwal PK (2013) A sensitivity study on the role of the swamps of southern Sudan in the summer climate of North Africa using a regional climate model. Theor Appl Climatol 113(1–2):63–81

Zhang C, Wang Y, Hamilton K (2011) Improved representation of boundary layer clouds over the Southeast Pacific in ARW-WRF using a modified Tiedtke cumulus parameterization scheme. Mon Weather Rev 139(11):3489–3513